Environment International 144 (2020) 106079

Contents lists available at ScienceDirect

Environment International

journal homepage: www.elsevier.com/locate/envint

Biomass burning organic aerosols significantly influence the light absorption properties of polarity-dependent organic compounds in the Pearl River Delta Region, China

Hongxing Jiang[a,d], Jun Li[a,*], Duohong Chen[b,*], Jiao Tang[a,d], Zhineng Cheng[a], Yangzhi Mo[a], Tao Su[a,d], Chongguo Tian[c], Bing Jiang[a], Yuhong Liao[a], Gan Zhang[a]

[a] State Key Laboratory of Organic Geochemistry and Guangdong province Key Laboratory of Environmental Protection and Resources Utilization, Guangzhou Institute of Geochemistry, Chinese Academy of Sciences, Guangzhou 510640, China
[b] Guangdong Environmental Monitoring Center, Guangzhou 510308, China
[c] Key Laboratory of Coastal Environmental Processes and Ecological Remediation, Yantai Institute of Coastal Zone Research, Chinese Academy of Sciences, Yantai 264003, China
[d] University of Chinese Academy of Sciences, Beijing 100049, China

ARTICLE INFO

Handling Editor: Xavier Querol

Keywords:
Brown carbon
Polar carbon fractions
Biomass burning organic aerosol
Pearl River Delta Region
Molecular composition

ABSTRACT

Atmospheric brown carbon (BrC) is an important constituent of light-absorbing organic aerosols with many unclear issues. Here, the light-absorption properties of BrC with different polarity characteristics at a regional site of Pearl River Delta Region during 2016–2017, influenced by sources and molecular compositions, were revealed using radiocarbon analysis and Fourier transform ion cyclotron resonance mass spectrometry. Humic-like substance (HULIS), middle polar (MP), and low polar (LP) carbon fractions constitute 46 ± 17%, 30 ± 7%, and 7 ± 3% of total absorption coefficient from bulk extracts, respectively. Our results show that the absorption proportions of HULIS and MP to the total BrC absorption are higher than their mass proportions to organic carbon mass, indicating that HULIS and MP are the main light-absorbing components in water-soluble and water-insoluble organic carbon fractions, respectively. With decreases in non-fossil HULIS, MP, and LP carbon fractions (66 ± 2%, 52 ± 2%, and 36 ± 3%, respectively), the abundances of unsaturated compounds and mass absorption efficiency at 365 nm of three fractions decreased synchronously. Increases in both non-fossil carbon and levoglucosan in winter imply that the enhanced light-absorption could be attributed to elevated levels of biomass burning organic aerosols (BBOA), which increases the number of light-absorbing nitrogen-containing compounds. Moreover, the major type of potential BrC in HULIS and MP carbon fractions are oxidized BBOA, but the potential BrC chromophores in LP are mainly associated with primary BBOA. This study reveals that biomass burning has adverse effects on radiative forcing and air quality, and probably indicates the significant influences of atmospheric oxidation reactions on the forms of chromophores.

1. Introduction

Organic carbon (OC) is an important component of atmospheric aerosols, and it has extremely significant effects on global climate change, radiative forcing, visibility, air quality, and human health (Jimenez et al., 2009; Ramanathan et al., 2005). Recently, a certain type of colored OC, termed atmospheric brown carbon (BrC), has been shown to absorb sunlight in the near ultraviolet–visible region and exhibit strongly wavelength-dependent absorbance (Andreae and Gelencsér, 2006; Hecobian et al., 2010; Wang et al., 2014). BrC has large impacts on regional climate and hydrological cycles, and causes large uncertainties when estimating radiative forcing (Moise et al., 2015; Ramanathan et al., 2005; Wang et al., 2014). Laboratory combustion, chamber simulation experiments, and field studies have demonstrated that both primary emissions, such as biomass burning (BB) (Chen and Bond, 2010; Cheng et al., 2016) and fossil fuel combustion (Healy et al., 2015; Li et al., 2018; Yan et al., 2017), and secondary organic aerosol (SOA) formation from biogenic (Nguyen et al., 2013; Xie et al., 2019) and anthropogenic (Liu et al., 2016a; Xie et al., 2017) volatile organic compounds (VOCs) can generate light-absorbing species.

The characterization of the composition, structure, and optical

* Corresponding authors.
E-mail addresses: junli@gig.ac.cn (J. Li), chenduohong@139.com (D. Chen).

https://doi.org/10.1016/j.envint.2020.106079
Received 16 June 2020; Received in revised form 13 August 2020; Accepted 19 August 2020
Available online 28 August 2020

properties of BrC can provide source information and estimate the effects of BrC on climate (Laskin et al., 2015). Presently, most studies on BrC in the literature have focused mainly on the absorption properties in various carbon fractions, molecular composition, as well as specific chromophores and their formation mechanisms. The solvent extract method provides an easy way to analyze the light absorption properties and chemical composition of aerosol. Many studies have shown that the amount of solar radiation absorbed by water-soluble organic carbon (WSOC) relative to elemental carbon (EC) is in the range of 1–14% over the whole solar spectrum (Huang et al., 2018; Kirillova et al., 2014a, 2014b; Yan et al., 2015), and in some biomass burning influenced regions such as Indo-Genic Plain, the ratio could up to 30–40% (Srinivas and Sarin, 2014, 2019). Additionally, studies have suggested that methanol has a higher BrC extraction efficiency than water (Chen and Bond, 2010; Cheng et al., 2016; Zhang et al., 2013a). Other than those polar BrC chromophores appearing in WSOC, methanol extracts contain water-insoluble absorbing compounds with less polarity, such as polycyclic aromatic hydrocarbons (PAHs) and O-heterocyclic and N-heterocyclic PAHs (Chen et al., 2017; Huang et al., 2018; Lin et al., 2018). In some previous studies, water-insoluble organic carbon (WISOC) even have higher light-absorption than that of WSOC (Chen et al., 2017; Zhang et al., 2013a). For example, Zhang et al. (2013a) found that the WISOC was highly absorbing and on average was 4.2 times more absorbing than WSOC at 365 nm. And Chen et al. (2017) have indicated that the relative contributions to the light absorption for WISOC increased from 250 nm to 600 nm, and dominant in the visible region. The authors attributed the strongly light-absorbing compounds in WISOC to large molecular weight PAHs, such as quinones.

Several advanced instruments have been used to characterize the molecular and structural composition of BrC. For example, Chen et al. (2016, 2017) conducted a series of experiments using Fourier transform infrared spectroscopy, nuclear magnetic resonance spectroscopy, and high-resolution aerosol mass spectrometry to investigate the relationships between optical properties and chemical structures of different organic components. The authors inferred that the light-absorption of organic aerosols are largely contributed by aromatic, oxygen- and nitrogen-containing compounds. However, the detailed information about chromophores and sources of these compounds in different organic components are rarely known. Most current studies investigating the influences of biomass burning events on water-soluble BrC composition have used high-resolution mass spectrometry. Their results showed that BB can obviously lead to the chromophores of nitro-containing compounds increase (Lin et al., 2017; Wang et al., 2019). The chromophoric organic compounds in WSOC are mainly aromatic carboxylic acid, phenols, and nitro-aromatics (Laskin et al., 2015; Moise et al., 2015). Several studies have determined that nitro-aromatics account for only 0.1–4% of total/water-soluble BrC light absorption at 365/370 nm in aerosol samples (Mohr et al., 2013; Teich et al., 2017; Zhang et al., 2013a); however, in cloud water samples, which are heavily affected by biomass burning, the nitro-phenols and aromatic carbonyl compounds can account for ~50% of BrC light absorption between 300 and 400 nm (Desyaterik et al., 2013). In WISOC, nevertheless, the water-insoluble BrC chromophores of PAHs and their derivatives only accounted ~1.7% to total BrC light absorption for ambient air samples (Huang et al., 2018), which is much lower than those of biomass burning organic aerosols (BBOA). Lin et al. (2018) have reported that PAHs and their derivatives are responsible for more than 40% of solvent-extractable BrC light absorption for fresh BBOA. Therefore, a large fraction of BrC chromophores has not been elucidated at present.

Generally, the sources of BrC were qualitatively characterized by tracer-based (e.g. levoglucosan) method and carbon isotopic method (Kirillova et al., 2014a; Wu et al., 2019; Yan et al., 2015). Many studies have exhibited that the BrC in the atmosphere have relations with the elevated BBOA. However, most previous knowledge about the BrC from these analyses only focus on the water-soluble BrC, while the effects of sources on the light-absorption properties and molecular composition of BrC in water-insoluble fractions are not well characterized.

In this study, combining with Fourier transform ion cyclotron resonance mass spectrometry (FT-ICR-MS) and radiocarbon (^{14}C) analysis, we aim to capture a better understanding of the effects of sources of atmospheric OC (include WSOC and WISOC) on light-absorption properties and chemical components. FT-ICR-MS, with its high resolution and accuracy, can be used to characterize the complete chemical composition of organic mixtures, e.g., humic-like substances (HULIS) (Mazzoleni et al., 2010; Song et al., 2018). The ^{14}C method is a powerful technique for analyzing source information related to fossil and non-fossil carbon origins. The Pearl River Delta region (PRD) is one of the most developed city clusters in China, with anthropogenic emissions heavily influencing atmospheric brown cloud formation in this area (Ramanathan et al., 2007). The objectives of this study were to investigate (1) the concentrations of and seasonal variation in polarity-dependent BrC in the PRD, (2) the molecular compositions and sources of major BrC fractions, and (3) the influence of BBOA on the BrC absorption of major BrC fractions.

2. Materials and methods

2.1. Sample collection and chemical separation

Field observations were conducted at the Guangdong Atmospheric Supersite, a semi-rural site located at Huaguo Shan (22.7279°N, 112.9290°E), southwest of the city of Heshan (HS), from May 2016 to April 2017. $PM_{2.5}$ samples were collected once each week using a prebaked quartz fiber filter (Munktell; MK360, 20.3 × 25.4 cm^2) over a period of 24 h with a high-volume air sampler (Shanghai XTrust Analytical Instruments Co., Ltd.) at a flow rate of 1 m^3/min. In total, 28 samples were collected, with six pieces of a filter punched out using a 22-mm-diameter steel filter punch for each sample (Table S1 in the Supporting Information). More details about the experimental strategies used to obtain the HULIS, MP, and LP carbon fractions are described in Text S1 in the Supporting Information. Briefly, the filter samples were first extracted using ultrapure water and then filtered to obtain the WSOC. Half of the WSOC was used for further HULIS isolation, and the carbon contents and light-absorption properties of non-HULIS were estimated by calculating the differences between WSOC and HULIS values (Lin et al., 2012a; Mo et al., 2018, 2017). After extracted by water, the rest of the filters were freeze-dried to avoid the interference of water in organic solvents extraction. The mixture of methanol/dichloromethane (MeOH/DCM = 1:1, v/v) was used for water-insoluble organic carbon (WISOC) extraction. The non-polar (NP), LP, and MP fractions were obtained via silica column chromatography separation with eluent solutions of n-hexane, n-hexane/DCM (1:2, v/v), and DCM/MeOH (1:2, v/v)–MeOH/$NH_3{\cdot}H_2O$ (wt 2%), respectively (Chen et al., 2017; Wozniak et al., 2012). In this study, the ratios of extracted carbon fractions (WSOC + MP + LP + NP) to total OC was 88 ± 19%. This ratio was very close to the result reported by previous study, which applied the similar analytical procedure (85 ± 6% and 106 ± 10%) (Chen et al., 2017). Therefore, we are satisfied to adopt that most of organic carbon were extracted by water and organic solvents.

2.2. UV–vis analysis

A UV–vis spectrophotometer (UNICO) was used for UV–vis absorption spectra measurements in the range of 250–800 nm at intervals of 0.5 nm with an accuracy of 10 nm. Quartz cells with a path length of 1 cm were used for placing the extracts. The corresponding blank solvent was scanned for baseline calibration before the absorption spectra of each type of solution were recorded. The absorbance of field blank sample extracts were all close to zero between 250 and 800 nm; thus, we did not have to perform subtractive work for blank correction.

Details of the calculation for light-absorption properties are provided in Text S2 in the Supporting Information. The absorption Ångström exponent (AAE) is widely used to describe the wavelength-dependence of BrC absorption and the values depend on the types of chromophores, which are related to sources and atmospheric processes (Li et al., 2016). Additionally, the mass absorption efficiency at 365 nm (MAE_{365}) is a useful parameter for extrapolating the optical properties and chemical composition of BrC.

2.3. Carbon contents, water-soluble ions, and organic tracer analysis

Details of the analysis methods for carbon contents, water-soluble ions (NH_4^+, K^+, Cl^-, SO_4^{2-}, and NO_3^-), and anhydrosugar isomers, i.e., levoglucosan, galactosan, and mannosan, are provided in Text S3 in the Supporting Information. Note that OC and EC levels in the filter samples were determined using an OC/EC analyzer (Sunset Laboratory, Inc.) with a flame ionization detector operated using the National Institute for Occupational Safety and Health thermal-optical transmittance standard method (NIOSH5040-TOT) (details described in Chen et al., 2009). The carbon contents of MP, LP, and NP, which dissolve in organic solvents, were analyzed based on a method described in previous studies (Chen et al., 2017; Cheng et al., 2012), and the carbon contents in WSOC and HULIS (in water) were measured using a total organic carbon analyzer (TOC-VCPH; Shimadzu) in triplicate with a relative procedural standard deviation of 0.83 mg/L. All sample quantities presented in this study were corrected using field blanks.

2.4. Electrospray ionization (ESI) FT-ICR-MS analysis

Solutions of polar carbon fractions (obtained with the method described above) from the same season were merged for FT-ICR-MS analysis. Samples were dried again under a gentle stream of nitrogen gas and then redissolved in 1 mL of MeOH for HULIS and MP or 1 mL of DCM for LP fractions before FT-ICR-MS analysis. The NP fraction, which was composed mainly of alkanes and exhibited almost no absorbance, was not analyzed using FT-ICR MS. Therefore, we focused only on polar fractions in this study. Samples were analyzed using a 9.4 T solariX XR FT-ICR-MS instrument (Bruker Daltonics GmbH) in the negative ESI mode (ESI−), and the detection mass range was set at 150–800 *m/z*. The instrument settings and calibration were similar to those described in previous studies (Jiang et al., 2016; Mo et al., 2018; Song et al., 2018). Field blank filters were processed and analyzed following the same procedures used for the samples, and blank data were subtracted from those of all samples. A custom software was used to calculate all mathematically possible formulae for all ions with a signal-to-noise ratio higher than 10 using a mass tolerance of ± 1.0 ppm. Additional details of the data processing procedure can be found in Text S4 in the Supporting Information. Note that a shortcoming of using the ESI− source is that light-absorbing less-polar compounds such as PAHs cannot be detected. However, the polar compounds are more easily detected because of easier ionization with an ESI− source (Lin et al., 2018).

2.5. Carbon isotope analysis

The samples selected for carbon isotopic analysis were the same as those used for FT-ICR-MS. Briefly, every six samples were selected to represent a season (Table S1 in the Supporting Information). The six samples were merged and subjected to the chemical procedures described above. HULIS, MP, and LP fractions were obtained and then concentrated to approximately 250 μL. For the radiocarbon measurements, after evaporating under a gentle flow of ultrapure N_2 for approximately 30–40 min, more than 200 μg of carbon was combusted into CO_2, cryogenically trapped, and then reduced into graphite targets for ^{14}C determination at the State Key Laboratory of Organic Geochemistry, Guangzhou Institute of Geochemistry, Guangzhou, China (Zhu et al., 2015). Detailed descriptions of the methods by which ^{14}C values were expressed and converted can be found in previous studies by our group (Liu et al., 2016b; Mo et al., 2018). Briefly, ^{14}C values were expressed as the fraction of modern carbon (f_m) after correcting for the $\delta^{13}C$ fractionation. The f_m value was further converted into fraction of non-fossil carbon (f_{nf}) using a correction factor of 1.052 based on the long-term time series of $^{14}CO_2$ sampled at the background station (Levin and Kromer, 2004; Levin et al., 2013). The carbon content in the field blanks was negligible, therefore, no field blank subtraction was performed for the isotope analysis in this study.

3. Results and discussion

3.1. Carbon-fraction and light-absorption properties

Table S2 summarizes the concentrations of bulk carbonaceous components, water-soluble ions, and three anhydrosugar isomers. The annual mean concentrations of OC, WSOC, HULIS, and MP, LP, and NP fractions were 8.09 ± 4.53, 3.83 ± 1.94, 2.08 ± 1.16, 1.77 ± 1.06, 0.67 ± 0.36, and 0.69 ± 0.29 μg C/m^3, respectively, with the highest values occurring in winter. Among the carbonaceous fractions, WSOC accounted for 50 ± 12% of the total OC content. HULIS is the major component and a strong light-absorbing component of WSOC, accounted for a mean of 54% of the WSOC annually. This proportion is similar to those reported by previous studies of the PRD (Fan et al., 2016; Kuang et al., 2015; Lin et al., 2010; Liu et al., 2018). However, the annual mean concentration of HULIS was 2.08 ± 1.12 μg C/m^3, which is close to or lower than the concentrations reported by the aforementioned studies. These results indicate that the concentration of HULIS varies widely, with spatial, temporal, and source differences (Zheng et al., 2013). Of the WISOC, the MP fraction was the major component, accounting for 23 ± 7% of the OC (Fig. S1). The LP and NP fractions accounted for similar percentages, both are ~10% of the OC. The relative contribution of the WISOC fractions (MP + LP + NP) to OC (~43%) is consistent with the result of a previous study that indicated that the difference between methanol-extracted OC and water-extracted OC can constitute approximately 45% of the OC mass (Cheng et al., 2016).

Fig. S2 and Fig. 1b show the absorption coefficients (Abs) of the WSOC, MP, LP, and NP fractions and their relative contributions to the total light absorption ($Abs_{Total} = Abs_{WSOC} + Abs_{MP} + Abs_{LP} + Abs_{NP}$) in the range of 250–600 nm. Our result revealed that the NP fraction has an extremely low absorption proportion in the near UV–vis spectrum, accounting for less than 1% in all samples. Thus, it is an unimportant light absorption constituent and can be overlooked (the same hereinafter). The major light absorption constituent, WSOC, accounts for about 60% of the total light absorption in the ultraviolet area and increases slightly in contribution with wavelength in the visible range. HULIS contributes an average of about 63% of the WSOC light absorption in the range of 250–600 nm and accounts for 42 ± 11% of the total BrC absorption at 365 nm, which is about two times higher than that of the non-HULIS component (21 ± 8%). The absorption contribution proportions of MP are relatively stable in the entire wavelength range, accounting for nearly one-third of the total light absorption. The absorption contributions of LP, which is usually considered to be aromatic fraction, shows a remarkable decrease from 10% at 250 nm to about 2% at 600 nm.

Our result is quiet similar with a previous study conducted by Chen et al. (2017) that MP was the major light-absorption fraction in WISOC using the similar method. However, their results showed that the WISOC accounted higher BrC absorption in the visible region (400–600 nm) than that of the WSOC, while the absorption of WSOC was dominant in the UV region (250–400 nm). This is different from our studies that WSOC was the major BrC component both in UV and visible region. In this study, the Abs_{365} of WISOC was 0.30–1.97 times of WSOC, with the mean value of 0.67 ± 0.35. Actually, the difference

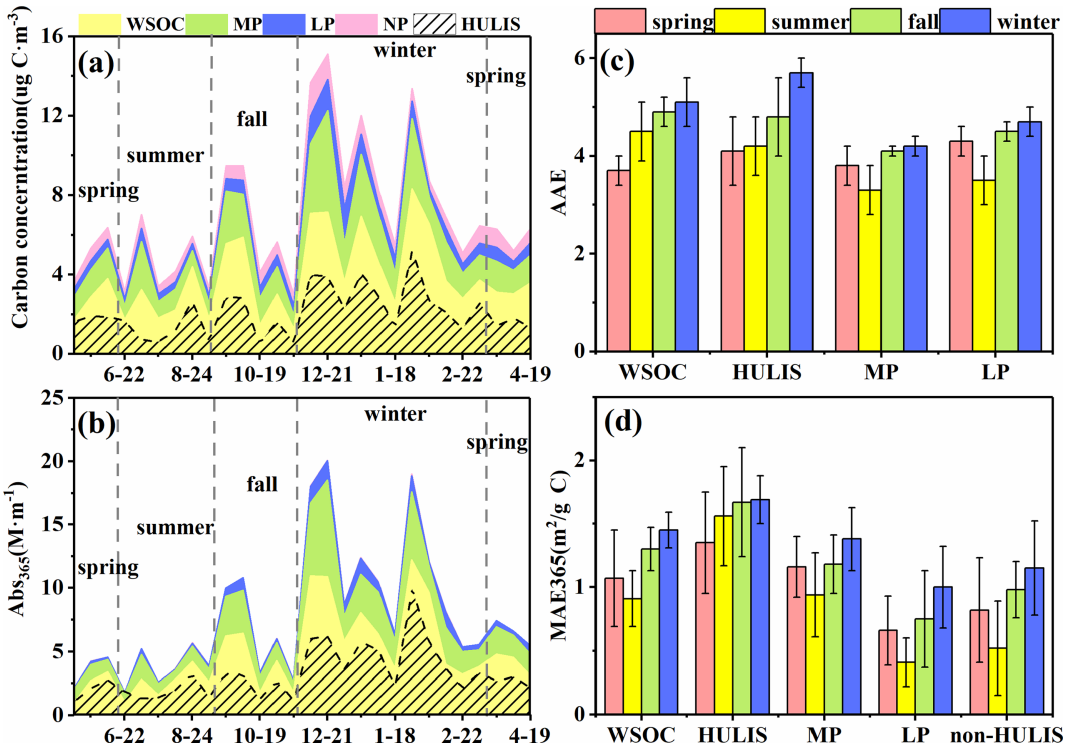

Fig. 1. Annual trends of carbon concentration (a), Abs_{365}(b) for WSOC, HULIS, MP, LP and NP fractions. (c) and (d) shows the seasonal variations of AAE and MAE_{365} for WSOC, HULIS, MP and LP fractions. Noted that the dash shadow area represents the portion of HULIS in WSOC.

in WSOC contribution to BrC absorption can be attributed to the spatial heterogeneity of emission sources and atmospheric processes. For example, Lin et al. (2017) also found a similar trend to ours for the before- and post-BB influenced aerosol samples in Rehovot. The authors declared the BrC in these samples are mainly composed by highly oxidized WSOC after comparing with the fresh BBOA samples. In Seoul (Kim et al., 2016), the light absorption contributed by WISOC showed a clear seasonal variations, with the dominant light-absorption contributed by WISOC in summer, while in other seasons, WSOC was the main contributors. The authors attributed it to that photochemically generated SOA from anthropogenic emissions seems to be the major source in summer, whereas aged/oxidized compounds were the major source in other seasons. Therefore, considering the high atmospheric oxidation level and relative humidity across the year in PRD (Ding et al., 2012), the higher light absorption of WSOC than WISOC in this study indicates the possibility of influences of aging and oxidization processes in the full year. (Gilardoni et al., 2016; Zhong and Jang, 2014)

3.2. Origins of major BrC components

The sources of HULIS, MP and LP fractions were characterized using tracer-based and ^{14}C methods. Pearson correlation analysis (Table S3) showed that HULIS and the MP fraction were significantly correlated ($r > 0.7$, $P < 0.01$) with anhydrosugars, indicating that BB has an important influence on these fractions. Secondary species (i.e., NH_4^+, NO_3^-, and SO_4^{2-}) were also moderately ($0.4 < r < 0.7$, $p < 0.05$) or well correlated ($r > 0.7$, $p < 0.05$) with the two fractions, which indicates the possible influences of anthropogenic SOA formation (Fig. S3). HULIS can be emitted directly as primary emissions (i.e., BB, fossil fuel combustion) and also be formed from SOAs from biogenic and anthropogenic emissions (Gao et al., 2006; Graber and Rudich, 2006; Lin et al., 2010). The LP fractions were weakly ($r < 0.5$, $P < 0.05$) or not correlated with anhydrosugars but were significantly correlated with species such as EC ($r = 0.66$, $P < 0.01$), K^+($r = 0.68$, $P < 0.01$), and SO_4^{2-} ($r = 0.60$, $P < 0.01$). Given that other than BB, K^+ has various sources such as sea salt and coal combustion (Li et al., 2019b). Our results indicate that the possibility influences of anthropogenic sources such as fossil fuel combustion to LP, while HULIS and MP fraction probably are mainly associated with BB and atmospheric SOA formation.

Radiocarbon analysis provided more specific information about the contributions of fossil and non-fossil carbon to the total OC. Although BrC only accounted a small fraction to extracted carbon fractions, however, our correlation analysis (Table S3) show that the BrC in each carbon fraction has same sources with their corresponding carbon fraction. In this study, the f_{nf} values of the three organic fractions were strongly polar-dependent with the following values: HULIS (0.63–0.68) > MP (0.50–0.54) > LP (0.32–0.39) (Fig. 2). In combination with the result of our group's previous study that non-HULIS have a larger non-fossil contribution (~8%) than HULIS (Mo et al., 2018), therefore, our results show that the BrC aerosols with more polar functional groups over PRD showed predominance of non-fossil origin. The high f_{nf} values associated with HULIS in our study provide further support for the fact that HULIS in the PRD are dominated by biogenic carbon, whereas the low f_{nf} values associated with the LP fraction indicate that it mainly originates from fossil fuel combustion-associated sources. Additionally, fossil and non-fossil sources play the same important roles in the formation of the MP fraction in the PRD. Note that the f_{nf} values associated with the MP and LP fractions were lower than those in rural areas (non-fossil carbon-dominant) (Wozniak et al., 2012) but higher than those of aerosols in urban areas (fossil carbon-dominant) (Currie et al., 1997) of the eastern USA, indicating that WISOC has different chemical compositions and sources between the PRD and those areas.

The f_{nf} values associated with HULIS, MP, and LP fractions show a clear seasonal trend with relatively low values occurring in summer (Fig. 2). Despite higher biogenic emissions and frequent SOA formation from biogenic VOCs in the summer season due to relatively high temperatures and strong solar radiation, lower BB emissions (low concentration of levoglucosan) and more wash-out processes may lead to

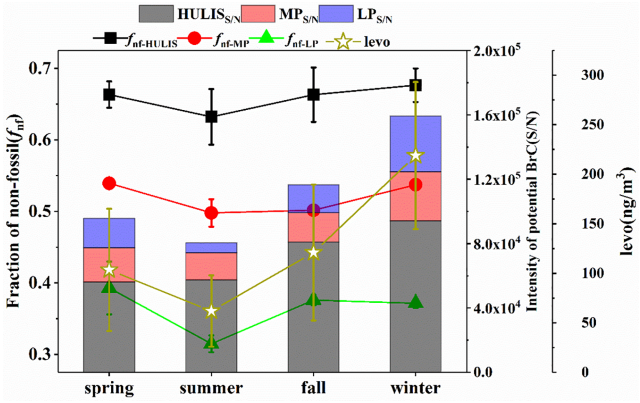

Fig. 2. Seasonal trends of concentration of levoglucosan (levo) and non-fossil fraction carbon in HULIS ($f_{nf\text{-}HULIS}$), MP ($f_{nf\text{-}MP}$) and LP ($f_{nf\text{-}LP}$). The colunm bar shows the seasonal varibility of sum intensity (S/N) of potentail BrC formulas detected in HULIS ($HULIS_{S/N}$), MP ($MP_{S/N}$) and LP ($LP_{S/N}$). The potentail BrC formula is selected based on the criteria of $0.5 \times c \leq DBE \leq 0.9 \times c$ (DBE: double bond equivalent, c: carbon numbers) which presented in Lin et al. (2018) Error bars represent the standard deviation of triplicate analysis for f_{nf} and the standard deviation of seasonal concentrations for levo.

low non-fossil contributions and overall low mass concentrations. However, the relative contributions of non-fossil HULIS, MP, and LP carbon fractions were fairly constant during spring, fall, and winter, but the absolute mass concentration of non-fossil carbon and the concentration of levoglucosan increased sharply in winter, indicating enhancement of BB emissions. Indeed, previous studies have reported that crop-burning events for agriculture and wood/charcoal burning for domestic heating occur widely during winter in South China (Liu et al., 2018; Qin et al., 2018; Zhang et al., 2013b).

3.3. Molecular composition of HULIS, MP, and LP fractions

3.3.1. General characterization

Due to the bias of ESI− for less polar and smaller molecules, only HULIS, MP, and LP fractions were analyzed using ESI-FT-ICR-MS. The reconstructed mass spectra are presented in Fig. S4. The mean numbers of detected formulas for the HULIS, MP, and LP fractions were 5415 ± 430, 3456 ± 867, and 2261 ± 739, respectively (Table S4). More species were detected in the polar fractions, similar to the results of WSOC contained more species than that observed for WISOC (Willoughby et al., 2014). The identified molecules were divided into four categories based on the elements in their molecular formulae: compounds only containing C, H, and O are assigned into CHO groups (similarly hereinafter). Significant differences in the HULIS, MP, and LP compositions are shown in the pie chart in Fig. S4. The peak intensity percentages associated with HULIS were very similar—CHONS, 25–33%; CHOS, 23–29%; CHO, 21–24%; and CHON, 18–26%. The CHO species were the most abundant in MP and LP fractions, accounting for 46–60% and 70–81% of the total intensity, respectively. In the similar study, Chen et al. (2017) also revealed that the relative abundance of the oxygenated compounds was polarity-dependent by various methods, which is consistent with our results. On the contrary, the abundances of sulfur-containing compounds (SOCs; CHOS + CHONS) were relatively low, only 27–35% for MP and 5–7% for LP. The reason for the low abundances of SOCs in the relatively weak polar fraction may be because SOCs such as organosulfates and sulfonates are more soluble in water. The abundances of CHON compounds in the MP and LP fractions were close to those in HULIS, which may indicate the wide polar range and complexity of the composition of nitro-containing compounds.

3.3.2. SOCs

The aromaticity index (AI) is used to improve the identification and characterization of aromatic and condensed aromatic compounds, and the ratio of double-bond equivalents value to carbon number (DBE/C) is related to the density of double bonds and their aromaticity (Koch and Dittmar, 2006; Lin et al., 2012a). In this study, more than 96% of SOCs had AI value lower than 0.5 for all HULIS and MP samples, and more than 94% of the CHOS compounds in the LP fraction had AI* < 0.5, which means that they were mainly composed by aliphatic/ olefinic organosulfates (Table S5). These sulfur-containing compounds are unlikely to be the main BrC chromophores. Although previous studies have shown that there is a large number of organosulfates in the fresh aerosols produced by engine emissions and coal combustion, those fresh organosulfates tend to be more aromatic with high AI and DBE/C values and probably were the product of thermal reactions of benzenes with SO_2 during combustion processes (Cui et al., 2019; Fan et al., 2019; Song et al., 2018). Therefore, the organosulfates detected in this study are more likely to be SOA products of VOCs, which are formed through the reaction of unsaturated and long-chain alkenes/fatty acids with SO_2 (He et al., 2014; Kuang et al., 2016; Lin et al., 2012b; Zhu et al., 2019).

3.3.3. CHON compounds

Many studies have shown that nitrogen-containing organic compounds (NOCs) such as N-heterocyclic compounds, nitrated phenols, and nitro-aromatic compounds are important BrC chromophores, and BB is one of the most important sources of NOCs (Claeys et al., 2012; Desyaterik et al., 2013; Lin et al., 2016; Mohr et al., 2013; Wang et al., 2019). However, the N-bases cannot be detected in ESI− mode. Here, the seasonal trend of the content of CHON compounds was same as that of the non-fossil sources, i.e., the highest contents of CHON compounds in HULIS, MP and LP fractions occurred in winter, implying a possible enhanced contribution of biomass burning. The O/N ratio of CHON compounds decreased with polarity in the order of HULIS > MP > LP fraction, indicating that the CHON compounds detected in LP fractions were less oxidized. According to previous studies, O/N ≥ 3 may indicate nitro (–NO_2) or nitrooxy (–ONO_2) compounds and O/N < 3 may indicate reduced N compounds (Laskin et al., 2009; Lin et al., 2012a). In this study, nitro compounds or organonitrates were the predominant components of CHON compounds, accounting for more than 90% of the total in HULIS and MP fractions and 70–87% in the LP fraction (Table S6). The abundance-weighted AI and DBE/C values (AI* and DBE/C*, abundance-weighted average values were marked by "$_*$") associated with CHON compounds indicate that there were more aromatic structures in HULIS (Table S4). For example, the AI* value associated with HULIS was usually higher than that associated with the MP or LP fraction. The double-bond equivalents (DBE) values associated with HULIS were in the range of 4–15, whereas a large number of compounds in MP and LP have DBE values lower than 4. The structures of molecules with high-intensity peaks observed in the analysis of different polar fractions may indicate the possible sources of CHON compounds. As shown in Fig. S5, high-intensity peaks arising from $C_8H_{11}NO_7$ and $C_7H_7NO_4$ with DBE values of 4 and 5, respectively, were detected in the HULIS analysis. $C_7H_7NO_4$ has been reported in many studies and is thought to be methyl-nitrocatechol, which is an important type of BrC chromophore related to secondary BBOA (Desyaterik et al., 2013; Lin et al., 2016, 2017; Mohr et al., 2013). In the MP fraction, the high-intensity peaks arising from $C_{12}H_7NO_4$ and $C_{13}H_7NO_4$ could represent potential BrC chromophores because they have high DBE values of 10 and 11. These compounds most likely to be the nitration products of naphthalene. The abundant nitrogen-heterocyclic species of $C_{16}H_{10}N_2O_2$, with a DBE value of 13, was detected in the LP fraction and tentatively assigned as indigo. Indigo is a natural plant pigment and mainly from *polygonum* (which is a kind of widely spread plant in China and growth everywhere in the farmland). The $C_{16}H_{10}N_2O_2$ detected in our samples are probably unintentionally emitted along with the opening biomass burning events, such as straw

combustion in the farmland. Moreover, all of these BrC candidate compounds exhibited an obvious seasonal trend, with a high intensity in winter and low intensity in summer, which is similar to the trend in levoglucosan concentrations, further proving the influence of BB on the molecular composition of CHON compounds (Fig. S6).

3.3.4. CHO compounds

The CHO compounds identified using FT-ICR-MS most probably bear carboxyl and hydroxyl groups. The ratios of O/C* and H/C* can reflect the oxidation and saturation states of each compound. In this study, the O/C* ratios of CHO in the HULIS, MP, and LP fractions were 0.39–0.43, 0.25–0.30, and 0.11–0.13, respectively, and the H/C* ratios in the three fractions were ranked in the following order: HULIS (1.21–1.30) < MP (1.41–1.52) < LP (1.58–1.72), indicating that the degree of oxidation/unsaturation decreased/increased with decreased polarity. The van Krevelen diagram can provide a better understanding of distinct structural properties among HULIS, MP, and LP fractions (Fig. S7). Many intense CHO compounds associated with the MP and LP fractions were observed in the region A of the diagram, with relatively high H/C* and low O/C* ratios, which are often attributed to aliphatic compounds such as fatty acids (Wozniak et al., 2008; Zuth et al., 2018), whereas the intense CHO compounds associated with HULIS were located in the lignin-like region, which represents compounds similar to the pyrolysis products of lignin. The diagram is consistent with previous results, indicating that HULIS is composed mainly of terpenoid acids and aromatic carboxylic acids (Laskin et al., 2015; Lin et al., 2012a; Zheng et al., 2013). In addition, many molecules found in the three carbon fractions were located in region B, rather than region A. Unsaturated hydrocarbons and polycyclic aromatic structures are often assigned to region B, and the formulae represented by this region may reflect the influence of anthropogenic sources (Kourtchev et al., 2014). Fig. S8 further shows the varying trends in DBE values according to increasing C number. The high-intensity CHO compounds in HULIS were mostly associated with a DBE range of 3–12 and a carbon number range of 5–20, whereas the high-intensity compounds in the MP and LP fractions were generally associated with DBE values of less than 5 and carbon number values of more than 14. Table S5 also lists that the relative contents of CHO compounds with AI < 0.5, which were generally ranked in the following order: HULIS < MP < LP. These results imply that the CHO molecules with lower polarity are composed of many higher molecular-weight compounds with a lower degree of unsaturation. It is worth noting that although the LP fraction usually is considered an aromatic fraction that contains PAHs, it could not be detected using the negative ESI ion-source mode employed in this study.

3.4. Linkages between light-absorption properties and molecular characteristics

A similar seasonal trend of AAE and MAE_{365} values was observed for all carbon fractions, with the highest values appearing in winter, as well as the higher average values in cold seasons than warm seasons, indicating possibly similar seasonal variations of BrC sources and chemical composition (Fig. 1c&d). In this study, the mean AAE values of HULIS (4.8 ± 0.9) and WSOC (4.6 ± 0.7) in the range of 330–400 nm (hereinafter the same) were close, and the AAE values of MP (3.9 ± 0.4) and LP (4.3 ± 0.6) were slightly lower than those of WSOC and HULIS. The MAE at 365 nm also showed distinct polarity variations in the descending order of HULIS (1.6 ± 0.4 $m^2 \cdot g^{-1}C$) > MP (1.2 ± 0.3 $m^2 \cdot g^{-1}C$) > non-HULIS (0.9 ± 0.4 $m^2 \cdot g^{-1}C$) > LP (0.8 ± 0.4 $m^2 \cdot g^{-1}C$) (The difference between these data have been tested by using one-way ANOVA with $p < 0.01$). We also calculated the MAE at 300–700 nm, which show similar descending trends with MAE at 365 nm for carbon fractions (Fig. S2). The stronger light-absorption capability exhibited by HULIS and MP than the other fractions probably demonstrates they contains more number of chromophores, which further indicates they are major light-absorbing components.

It is worth noting that the light absorption capacities of BrC usually related with the aromaticities and degree of conjugation (Laskin et al., 2015). Atmospheric aging processes also can lead to the enhancement or photochemical degradation of BrC absorption via changing the molecular composition, such as O/C ratios (Lambe et al., 2013; Lee et al., 2014). As shown in Table S4, relative abundance-weighted H/C*, O/C*, DBE/C* and AI* values in the four categories representing the three fractions were usually polarity dependent. The O/C*, AI* and DBE/C* values in each HULIS compound category were significantly higher than those of the MP and LP fractions, which is similar to the trend of MAE_{365}. This probably means that the light-absorption capability of the three fractions was associated with the diversity of oxidation levels and aromaticities. Additionally, AI* and DBE/C* values associated with CHON were generally higher than those associated with the CHO categories, and the SOCs had the lowest AI* and DBE/C* values, indicating more double-bond structures in CHON groups.

3.5. Influence of BBOA on BrC molecular composition and absorption

The light-absorption properties of BrC can be affected by various factors. In general, the light-absorption capacity of BrC is directly related to the molecular composition of the bulk components, which is usually influenced by different sources and atmospheric processes. Abs_{365} is a key parameter that can be used to describe the absorption of BrC and is used as a proxy of BrC during extraction. The Pearson correlation coefficients for the associations between Abs_{365} and HULIS, MP, and LP fractions, as well as EC, levoglucosan, and water-soluble ions are shown in Table S3 and Fig. S9. Significantly positive correlations were observed between Abs_{365} of each carbon fraction and levoglucosan ($r > 0.71$, $P < 0.01$, $n = 20$, 8 missing values were precluded) and K^+ ($r > 0.78$, $P < 0.01$, $n = 28$), indicating that BB may have significant effects on BrC in the three carbon fractions. Furthermore, the Abs_{365} of each carbon fraction also show moderately or well correlations with EC (tracer of incomplete combustion) and anthropogenic ions (e.g. NO_3^-, SO_4^{2-} and NH_4^+), implying the possible influence of anthropogenic fossil fuel combustion (e.g., coal, gasoline, or diesel) on BrC in all three carbon fractions (Wu et al., 2019).

Additionally, the consistent seasonal trends in MAE_{365}, f_{nf}, and levoglucosan for all carbon fractions, with higher values in winter (Figs. 1 and 2), indicating that the increase in BrC absorption in winter may also be caused by more BB emissions. Furthermore, the significant positive correlation between MAE_{365} and f_{nf} ($r = 0.93$, $p < 0.01$) in the three fractions in different seasons indicates that BB plays a predominant role in the BrC absorption of atmospheric aerosols in the PRD (Fig. 3a). As shown in Fig. 3b, MAE_{365} values were positively correlated with DBE/C* values ($r = 0.93$, $p < 0.01$), suggesting that the increased BB emissions led to the high density of double bonds in molecular composition, which induced the relatively strong BrC absorption. To avoid interference from aliphatic compounds, which would likely not be BrC chromophores, molecule types with DBE values in the range of $0.5 \times c \leq DBE \leq 0.9 \times c$ (c, carbon number) were selected as potential BrC chromophores (Lin et al., 2018). Significant positive correlations were observed between MAE_{365} values and the total selected potential BrC formula number ($r = 0.97$, $p < 0.01$) (Fig. 3c). The percentage intensity in each category of BrC relative to those of all identified formulae (Int_C/Int_{bulk}) are also shown in Table S7. For HULIS, MP, and LP fractions, the Int_C/Int_{bulk} ratios of CHON in winter increased to almost 2–3-fold of those in summer (HULIS, 0.08 vs. 0.15; MP fraction, 0.06 vs. 0.13; LP fraction, 0.02 vs. 0.6), whereas the Int_C/Int_{bulk} ratios of SOCs did not exhibit obvious seasonal variations. As shown in Fig. 3d, significant positive correlations were observed between MAE_{365} values and the relative contents of potential CHON BrC ($r = 0.88$, $p < 0.01$), confirming that variation in BrC absorption is mainly affected by N-containing compounds. Aside from the potential

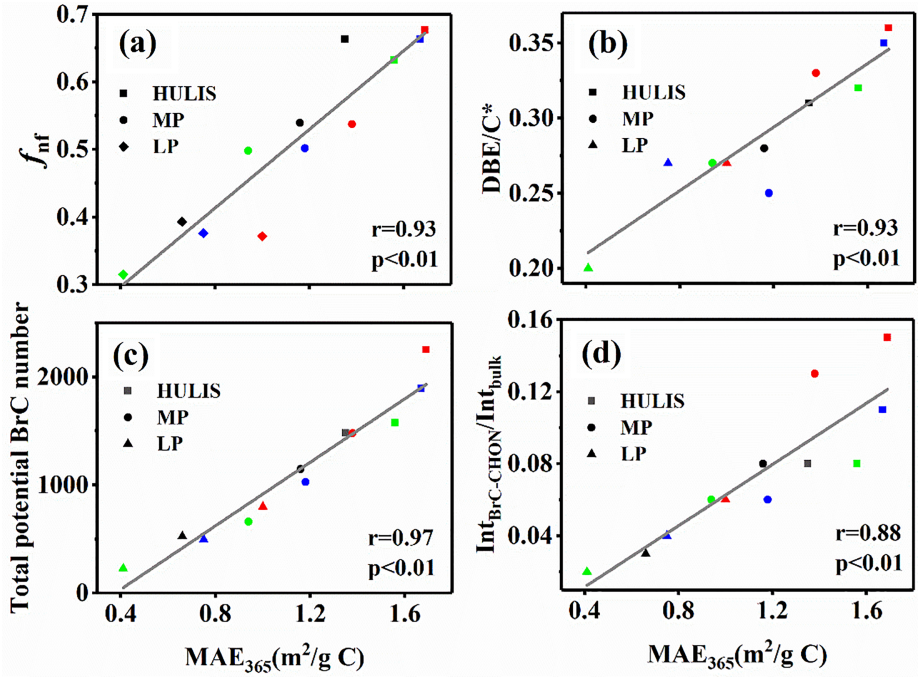

Fig. 3. Correlation between the MAE_{365} values and the fraction of non-fossil carbon (a), relative abundance-weighted DBE/C* (b), total number of potential BrC formuals (c), and relative content of potential BrC for CHON ($Int_{BrC-CHON}/Int_{bulk}$) (d). The box, circle and triangle denote the carbon fractions of HULIS, MP and LP, respectively. Color: black (spring), green (summer), bule (fall) and red (winter). (For interpretation of the references to color in this figure legend, the reader is referred to the web version of this article.)

CHON BrC, the light-absorbing CHO compounds in the LP fraction also increased greatly (from 0.06 to 0.13). For example, there was a sharp increase in the intensity of $C_{19}H_{10}O_2$ (S/N increased from 36 in summer to 384 in winter), which has been detected in freshly emitted BBOA (Lin et al., 2016). It should be noted that the light-absorbing CHO compounds in the LP fraction were associated with AI* ≥ 0.67 (Table S7), which indicates that the BrC comprising CHO compounds from BBOA is more likely to be compounds exhibiting high aromaticity and lower polarity, such as oxidized-PAHs (Lin et al., 2018).

Combining with the source analysis, we found that the BrC in winter at PRD was mainly affected by biomass burning, which is characterized by light-absorption nitrogen-containing compounds (including a large number of unique nitrogen compounds) and most of them with higher oxidation levels (O/N ratios ≥3) can be attributed to nitro- compounds or organonitrates. Previous studies indicate that although the fresh-emitted BBOA also contains nitro-aromatic compounds, the main chromophore is aromatic compounds containing the hydroxyl/methoxy or aldehyde/ketone group (Lin et al., 2016, 2017). Recent simulation experiments have confirmed that secondary nitrogen-containing BrC can be formed in BBOA under the presence of NOx (Li et al., 2019a). Therefore, we speculate that the light-absorbing nitrogen-containing chromophores detected in winter (high concentration of NO_3^-) at PRD area, are likely to be the secondary products of BBOA after atmospheric oxidation processes (i.e. nitration process). Also, we noted that the possibly transformation of compounds from relative lower polar to higher polar via functionalization (the oxidative addition of polar functional groups to the carbon skeleton) was shown in the Kroll plot (Fig. S11) (Kroll et al., 2011). For example, the tentatively identified formulas of $C_{10}H_7NO_{3\text{-}7}$, $C_{11}H_9NO_{3\text{-}7}$ and $C_{12}H_{11}NO_{3\text{-}7}$ with relatively high intensity detected in MP probably are oxidized products of PAHs (naphthalene); and the tentatively identified formulas of $C_7H_7NO_{4\text{-}5}$, $C_8H_7NO_{3\text{-}7}$, $C_9H_7NO_{3\text{-}7}$, $C_9H_9NO_{3\text{-}7}$ detected in HULIS probably are oxidized products of phenols (Lin et al., 2017). Therefore, our results probably imply that oxidation processes in atmosphere makes the chemical composition of BrC less diverse, more persistent and hydrophilic.

4. Conclusions

This study reports the seasonal variations in light absorption properties and sources of polar-dependent organic fractions at a typically regional site of the PRD, which include the high polar fraction of HULIS in WSOC, as well as the middle polar(MP) and low polar(LP) carbon fractions in WISOC. The results highlight that the MAE_{365} values of the three carbon fractions are well polar-dependent, which shows similar trends with the average AI and DBE/C values but opposite to the proportions of CHO compounds. Carbon isotopic compositions of polar-dependent organic fractions, supplemented with FT-ICR-MS, major ions and organic tracers, indicate that the significant influences of biomass burning to the BrC absorption of HULIS, MP and LP, although the major components and sources of these carbon fractions are obviously distinct. The MAE_{365} of BrC absorption in winter increased to as high as 1.08–2.44 times of those in summer for different polar carbon fractions, and the absolute fossil and non-fossil carbon content in winter increased to as high as 1.91–2.10 and 2.33–2.70 times of those in summer, respectively. Moreover, the relative content of the potential light-absorbing nitrogen-containing compounds also increased, with the content increasing 2–3 times in biomass burning influenced seasons than in summer. This result imply that biomass burning aerosols are important to the BrC seasonal variations both in rural and urban region (mainly affected by anthropogenic emissions, e.g. coal combustion and vehicle emissions). The BrC absorption generally enhanced along with the frequent haze explosion during the harvest and cold seasons in the Northern Hemisphere, which partially due to the elevated BB events for open agricultural residues burning and domestic heating. In the cold and dry days, the elevated BC and BrC absorb more sunlight and warm the air, which easily caused the formation of inversion layer and descending of boundary layer. Under these conditions, the more frequent SOA formations of anthropogenic emissions would aggravate the haze formations. Hence, controlling regional biomass combustion would be one of the effective ways to reduce regional air pollution.

CRediT authorship contribution statement

Hongxing Jiang: Writing - original draft, Visualization, Data curation. **Jun Li:** Validation, Investigation, Data curation, Writing -

review & editing, Project administration, Funding acquisition. **Duohong Chen:** Conceptualization, Supervision. **Jiao Tang:** Methodology, Data curation. **Zhineng Cheng:** Methodology, Data curation. **Yangzhi Mo:** Methodology, Data curation. **Tao Su:** Methodology, Data curation. **Chongguo Tian:** Data curation, Methodology, Writing - review & editing. **Bing Jiang:** Methodology, Data curation. **Yuhong Liao:** Methodology, Data curation. **Gan Zhang:** Investigation, Resources, Conceptualization, Writing - review & editing, Project administration, Funding acquisition.

Declaration of Competing Interest

The authors declare that they have no known competing financial interests or personal relationships that could have appeared to influence the work reported in this paper.

Acknowledgments

This study was supported by the National Key R&D Program of China (2017YFC0212000), National Natural Science Foundation of China (NSFC; Nos. 41773120), State Key Laboratory of Organic Geochemistry, GIGCAS (Grant No. SKLOG 2016-A05 and SKLOG 2020-5), and Guangdong Foundation for Program of Science and Technology Research (Grant No. 2017B030314057). The authors declare no competing financial interest. The data used in the paper is available at Harvard Dataverse (https://dataverse.harvard.edu/dataset.xhtml?persistentId=doi:10.7910/DVN/ONS2EY).

Appendix A. Supplementary material

Supplementary data to this article can be found online at https://doi.org/10.1016/j.envint.2020.106079.

References

Andreae, M.O., Gelencsér, A., 2006. Black carbon or brown carbon? The nature of light-absorbing carbonaceous aerosols. Atmos. Chem. Phys. 6, 3131–3148.
Chen, Q., Ikemori, F., Mochida, M., 2016. Light absorption and excitation-emission fluorescence of urban organic aerosol components and their relationship to chemical structure. Environ. Sci. Technol. 50, 10859–10868.
Chen, Q., Ikemori, F., Nakamura, Y., Vodicka, P., Kawamura, K., Mochida, M., 2017. Structural and light-absorption characteristics of complex water-insoluble organic mixtures in urban submicrometer aerosols. Environ. Sci. Technol. 51, 8293–8303.
Chen, Y., Bond, T.C., 2010. Light absorption by organic carbon from wood combustion. Atmos. Chem. Phys. 10, 1773–1787.
Chen, Y., Zhi, G., Feng, Y., Liu, D., Zhang, G., Li, J., Sheng, G., Fu, J., 2009. Measurements of black and organic carbon emission factors for household coal combustion in china: implication for emission reduction. Environ. Sci. Technol. 43, 9495–9500.
Cheng, Y., He, K., Du, Z., Engling, G., Liu, J., Ma, Y., Zheng, M., Weber, R.J., 2016. The characteristics of brown carbon aerosol during winter in Beijing. Atmos. Environ. 127, 355–364.
Cheng, Y., He, K., Duan, F., Du, Z., Zheng, M., Ma, Y., 2012. Characterization of carbonaceous aerosol by the stepwise-extraction thermal–optical-transmittance (SE-TOT) method. Atmos. Environ. 59, 551–558.
Claeys, M., Vermeylen, R., Yasmeen, F., Gómez-González, Y., Chi, X., Maenhaut, W., Mészáros, T., Salma, I., 2012. Chemical characterisation of humic-like substances from urban, rural and tropical biomass burning environments using liquid chromatography with UV/vis photodiode array detection and electrospray ionisation mass spectrometry. Environ. Chem. 9, 273.
Cui, M., Li, C., Chen, Y., Zhang, F., Li, J., Jiang, B., Mo, Y., Li, J., Yan, C., Zheng, M., Xie, Z., Zhang, G., Zheng, J., 2019. Molecular characterization of polar organic aerosol constituents in off-road engine emissions using Fourier transform ion cyclotron resonance mass spectrometry (FT-ICR MS): implications for source apportionment. Atmos. Chem. Phys. 19, 13945–13956.
Currie, L.A., Eglinton, T.I., Benner, B.A., Pearson, A., 1997. Radiocarbon “dating” of individual chemical compounds in atmospheric aerosol: first results comparing direct isotopic and multivariate statistical apportionment of specific polycyclic aromatic hydrocarbons. Nucl. Instrum. Meth. B 123, 475–486.
Desyaterik, Y., Sun, Y., Shen, X., Lee, T., Wang, X., Wang, T., Collett, J.L., 2013. Speciation of “brown” carbon in cloud water impacted by agricultural biomass burning in eastern China. J. Geophys. Res.: Atmos. 118, 7389–7399.
Ding, X., Wang, X.-M., Gao, B., Fu, X.-X., He, Q.-F., Zhao, X.-Y., Yu, J.-Z., Zheng, M., 2012. Tracer-based estimation of secondary organic carbon in the Pearl River Delta, south China. J. Geophys. Res.: Atmos. 117.
Fan, X., Song, J., Peng, P.A., 2016. Temporal variations of the abundance and optical properties of water soluble Humic-Like Substances (HULIS) in PM2.5 at Guangzhou, China. Atmos. Res. 172–173, 8–15.
Fan, X., Yu, X., Wang, Y., Xiao, X., Li, F., Xie, Y., Wei, S., Song, J., Peng, P.A., 2019. The aging behaviors of chromophoric biomass burning brown carbon during dark aqueous hydroxyl radical oxidation processes in laboratory studies. Atmos. Environ. 205, 9–18.
Gao, S., Surratt, J.D., Knipping, E.M., Edgerton, E.S., Shahgholi, M., Seinfeld, J.H., 2006. Characterization of polar organic components in fine aerosols in the southeastern United States: Identity, origin, and evolution. J. Geophys. Res. 111, D14314.
Gilardoni, S., Massoli, P., Paglione, M., Giulianelli, L., Carbone, C., Rinaldi, M., Decesari, S., Sandrini, S., Costabile, F., Gobbi, G.P., Pietrogrande, M.C., Visentin, M., Scotto, F., Fuzzi, S., Facchini, M.C., 2016. Direct observation of aqueous secondary organic aerosol from biomass-burning emissions. Proc. Natl. Acad. Sci. U. S. A. 113, 10013.
Graber, E.R., Rudich, A.Y., 2006. Atmospheric HULIS: How humic-like are they? A comprehensive and critical review. Atmos. Chem. Phys. 6, 729–753.
He, Q.F., Ding, X., Wang, X.M., Yu, J.Z., Fu, X.X., Liu, T.Y., Zhang, Z., Xue, J., Chen, D.H., Zhong, L.J., Donahue, N.M., 2014. Organosulfates from pinene and isoprene over the Pearl River Delta, South China: seasonal variation and implication in formation mechanisms. Environ. Sci. Technol. 48, 9236–9245.
Healy, R.M., Wang, J.M., Jeong, C.H., Lee, A.K.Y., Willis, M.D., Jaroudi, E., Zimmerman, N., Hilker, N., Murphy, M., Eckhardt, S., Stohl, A., Abbatt, J.P.D., Wenger, J.C., Evans, G.J., 2015. Light-absorbing properties of ambient black carbon and brown carbon from fossil fuel and biomass burning sources. J. Geophys. Res.: Atmos. 120, 6619–6633.
Hecobian, A., Zhang, X., Zheng, M., Frank, N., Edgerton, E.S., Weber, R.J., 2010. Water-Soluble Organic Aerosol material and the light-absorption characteristics of aqueous extracts measured over the Southeastern United States. Atmos. Chem. Phys. 10, 5965–5977.
Huang, R.J., Yang, L., Cao, J.J., Chen, Y., Chen, Q., Li, Y., Duan, J., Zhu, C., Dai, W., Wang, K., Lin, C., Ni, H., Corbin, J.C., Wu, Y., Zhang, R., Tie, X., Hoffmann, T., O'Dowd, C., Dusek, U., 2018. Brown carbon aerosol in urban Xi'an, Northwest China: the composition and light absorption properties. Environ. Sci. Technol. 52, 6825–6833.
Jiang, B., Kuang, B.Y., Liang, Y., Zhang, J., Huang, X.H.H., Xu, C., Yu, J.Z., Shi, Q., 2016. Molecular composition of urban organic aerosols on clear and hazy days in Beijing: a comparative study using FT-ICR MS. Environ. Chem. 13, 888.
Jimenez, J.L., Canagaratna, M.R., Donahue, N.M., Prevot, A.S.H., Zhang, Q., Kroll, J.H., DeCarlo, P.F., Allan, J.D., Coe, H., Ng, N.L., Aiken, A.C., Docherty, K.S., Ulbrich, I.M., Grieshop, A.P., Robinson, A.L., Duplissy, J., Smith, J.D., Wilson, K.R., Lanz, V.A., Hueglin, C., Sun, Y.L., Tian, J., Laaksonen, A., Raatikainen, T., Rautiainen, J., Vaattovaara, P., Ehn, M., Kulmala, M., Tomlinson, J.M., Collins, D.R., Cubison, M.J., Dunlea, J., Huffman, J.A., Onasch, T.B., Alfarra, M.R., Williams, P.I., Bower, K., Kondo, Y., Schneider, J., Drewnick, F., Borrmann, S., Weimer, S., Demerjian, K., Salcedo, D., Cottrell, L., Griffin, R., Takami, A., Miyoshi, T., Hatakeyama, S., Shimono, A., Sun, J.Y., Zhang, Y.M., Dzepina, K., Kimmel, J.R., Sueper, D., Jayne, J.T., Herndon, S.C., Trimborn, A.M., Williams, L.R., Wood, E.C., Middlebrook, A.M., Kolb, C.E., Baltensperger, U., Worsnop, D.R., 2009. Evolution of organic aerosols in the atmosphere. Science 326, 1525.
Kim, H., Kim, J.Y., Jin, H.C., Lee, J.Y., Lee, S.P., 2016. Seasonal variations in the light-absorbing properties of water-soluble and insoluble organic aerosols in Seoul, Korea. Atmos. Environ. 129, 234–242.
Kirillova, E.N., Andersson, A., Han, J., Lee, M., Gustafsson, Ö., 2014a. Sources and light absorption of water-soluble organic carbon aerosols in the outflow from northern China. Atmos. Chem. Phys. 14, 1413–1422.
Kirillova, E.N., Andersson, A., Tiwari, S., Srivastava, A.K., Bisht, D.S., Gustafsson, Ö., 2014b. Water-soluble organic carbon aerosols during a full New Delhi winter: isotope-based source apportionment and optical properties. J. Geophys. Res.: Atmos. 119, 3476–3485.
Koch, B.P., Dittmar, T., 2006. From mass to structure: an aromaticity index for high-resolution mass data of natural organic matter. Rapid Commun. Mass Spectrom. 20, 926–932.
Kourtchev, I., O'Connor, I.P., Giorio, C., Fuller, S.J., Kristensen, K., Maenhaut, W., Wenger, J.C., Sodeau, J.R., Glasius, M., Kalberer, M., 2014. Effects of anthropogenic emissions on the molecular composition of urban organic aerosols: an ultrahigh resolution mass spectrometry study. Atmos. Environ. 89, 525–532.
Kroll, J.H., Donahue, N.M., Jimenez, J.L., Kessler, S.H., Canagaratna, M.R., Wilson, K.R., Altieri, K.E., Mazzoleni, L.R., Wozniak, A.S., Bluhm, H., Mysak, E.R., Smith, J.D., Kolb, C.E., Worsnop, D.R., 2011. Carbon oxidation state as a metric for describing the chemistry of atmospheric organic aerosol. Nat. Chem. 3, 133–139.
Kuang, B.Y., Lin, P., Hu, M., Yu, J.Z., 2016. Aerosol size distribution characteristics of organosulfates in the Pearl River Delta region. China. Atmos. Environ. 130, 23–35.
Kuang, B.Y., Lin, P., Huang, X.H.H., Yu, J.Z., 2015. Sources of humic-like substances in the Pearl River Delta, China: positive matrix factorization analysis of PM2.5 major components and source markers. Atmos. Chem. Phys. 15, 1995–2008.
Lambe, A.T., Cappa, C.D., Massoli, P., Onasch, T.B., Forestieri, S.D., Martin, A.T., Cummings, M.J., Croasdale, D.R., Brune, W.H., Worsnop, D.R., Davidovits, P., 2013. Relationship between oxidation level and optical properties of secondary organic aerosol. Environ. Sci. Technol. 47, 6349–6357.
Laskin, A., Laskin, J., Nizkorodov, S.A., 2015. Chemistry of atmospheric brown carbon. Chem. Rev. 115, 4335–4382.
Laskin, A., Smith, J.S., Laskin, J., 2009. Molecular characterization of nitrogen-containing organic compounds in biomass burning aerosols using high-resolution mass spectrometry. Environ. Sci. Technol. 43, 3764–3771.
Lee, H.J., Aiona, P.K., Laskin, A., Laskin, J., Nizkorodov, S.A., 2014. Effect of solar radiation on the optical properties and molecular composition of laboratory proxies of atmospheric brown carbon. Environ. Sci. Technol. 48, 10217–10226.

Levin, I., Kromer, B., 2004. The tropospheric 14CO2 level in mid-latitudes of the northern hemisphere (1959–2003). Radiocarbon 46, 1261–1272.
Levin, I., Kromer, B., Hammer, S., 2013. Atmospheric Δ14CO2 trend in Western European background air from 2000 to 2012. Tellus B 65. https://doi.org/10.3402/tellusb.v3465i3400.20092.
Li, C., Chen, P., Kang, S., Yan, F., Hu, Z., Qu, B., Sillanpää, M., 2016. Concentrations and light absorption characteristics of carbonaceous aerosol in PM 2.5 and PM 10 of Lhasa city, the Tibetan Plateau. Atmos. Environ. 127, 340–346.
Li, C., He, Q., Hettiyadura, A.P.S., Kafer, U., Shmul, G., Meidan, D., Zimmermann, R., Brown, S.S., George, C., Laskin, A., Rudich, Y., 2019a. Formation of secondary brown carbon in biomass burning aerosol proxies through NO3 radical reactions. Environ. Sci. Technol. 54, 1395–1405.
Li, M., Fan, X., Zhu, M., Zou, C., Song, J., Wei, S., Jia, W., Peng, P., 2018. Abundances and light absorption properties of brown carbon emitted from residential coal combustion in China. Environ. Sci. Technol. 53, 595–603.
Li, Z., Tan, H., Zheng, J., Liu, L., Qin, Y., Wang, N., Li, F., Li, Y., Cai, M., Ma, Y., Chan, C.K., 2019b. Light absorption properties and potential sources of particulate brown carbon in the Pearl River Delta region of China. Atmos. Chem. Phys. 19, 11669–11685.
Lin, P., Aiona, P.K., Li, Y., Shiraiwa, M., Laskin, J., Nizkorodov, S.A., Laskin, A., 2016. Molecular characterization of brown carbon in biomass burning aerosol particles. Environ. Sci. Technol. 50, 11815–11824.
Lin, P., Bluvshtein, N., Rudich, Y., Nizkorodov, S.A., Laskin, J., Laskin, A., 2017. Molecular chemistry of atmospheric brown carbon inferred from a nationwide biomass burning event. Environ. Sci. Technol. 51, 11561–11570.
Lin, P., Engling, G., Yu, J.Z., 2010. Humic-like substances in fresh emissions of rice straw burning and in ambient aerosols in the Pearl River Delta Region. China. Atmos. Chem. Phys. 10, 6487–6500.
Lin, P., Fleming, L.T., Nizkorodov, S.A., Laskin, J., Laskin, A., 2018. Comprehensive molecular characterization of atmospheric brown carbon by high resolution mass spectrometry with electrospray and atmospheric pressure photoionization. Anal. Chem. 90, 12493–12502.
Lin, P., Rincon, A.G., Kalberer, M., Yu, J.Z., 2012a. Elemental composition of HULIS in the pearl river delta region, China: results inferred from positive and negative electrospray high resolution mass spectrometric data. Environ. Sci. Technol. 46, 7454–7462.
Lin, P., Yu, J.Z., Engling, G., Kalberer, M., 2012b. Organosulfates in humic-like substance fraction isolated from aerosols at seven locations in East Asia: a study by ultra-high-resolution mass spectrometry. Environ. Sci. Technol. 46, 13118–13127.
Liu, J., Lin, P., Laskin, A., Laskin, J., Kathmann, S.M., Wise, M., Caylor, R., Imholt, F., Selimovic, V., Shilling, J.E., 2016a. Optical properties and aging of light-absorbing secondary organic aerosol. Atmos. Chem. Phys. 16, 12815–12827.
Liu, J., Mo, Y., Ding, P., Li, J., Shen, C., Zhang, G., 2018. Dual carbon isotopes ((14)C and (13)C) and optical properties of WSOC and HULIS-C during winter in Guangzhou, China. Sci. Total Environ. 633, 1571–1578.
Liu, J., Mo, Y., Li, J., Liu, D., Shen, C., Ding, P., Jiang, H., Cheng, Z., Zhang, X., Tian, C., Chen, Y., Zhang, G., 2016b. Radiocarbon-derived source apportionment of fine carbonaceous aerosols before, during, and after the 2014 Asia-Pacific Economic Cooperation (APEC) summit in Beijing, China. J. Geophys. Res.: Atmos. 121, 4177–4187.
Mazzoleni, L.R., Ehrmann, B.M., Shen, X., Marshall, A.G., Collett, J.L., 2010. Water-soluble atmospheric organic matter in fog: exact masses and chemical formula identification by ultrahigh-resolution Fourier transform ion cyclotron resonance mass spectrometry. Environ. Sci. Technol. 44, 3690–3697.
Mo, Y., Li, J., Jiang, B., Su, T., Geng, X., Liu, J., Jiang, H., Shen, C., Ding, P., Zhong, G., Cheng, Z., Liao, Y., Tian, C., Chen, Y., Zhang, G., 2018. Sources, compositions, and optical properties of humic-like substances in Beijing during the 2014 APEC summit: Results from dual carbon isotope and Fourier-transform ion cyclotron resonance mass spectrometry analyses. Environ. Pollut. 239, 322–331.
Mo, Y., Li, J., Liu, J., Zhong, G., Cheng, Z., Tian, C., Chen, Y., Zhang, G., 2017. The influence of solvent and pH on determination of the light absorption properties of water-soluble brown carbon. Atmos. Environ. 161, 90–98.
Mohr, C., Lopez-Hilfiker, F.D., Zotter, P., Prevot, A.S., Xu, L., Ng, N.L., Herndon, S.C., Williams, L.R., Franklin, J.P., Zahniser, M.S., Worsnop, D.R., Knighton, W.B., Aiken, A.C., Gorkowski, K.J., Dubey, M.K., Allan, J.D., Thornton, J.A., 2013. Contribution of nitrated phenols to wood burning brown carbon light absorption in Detling, United Kingdom during winter time. Environ. Sci. Technol. 47, 6316–6324.
Moise, T., Flores, J.M., Rudich, Y., 2015. Optical properties of secondary organic aerosols and their changes by chemical processes. Chem. Rev. 115, 4400–4439.
Nguyen, T.B., Laskin, A., Laskin, J., Nizkorodov, S.A., 2013. Brown carbon formation from ketoaldehydes of biogenic monoterpenes. Faraday Discussions 165, 473.
Qin, Y.M., Tan, H.B., Li, Y.J., Li, Z.J., Schurman, M.I., Liu, L., Wu, C., Chan, C.K., 2018. Chemical characteristics of brown carbon in atmospheric particles at a suburban site near Guangzhou, China. Atmos. Chem. Phys. 18, 16409–16418.
Ramanathan, V., Chung, C., Kim, D., Bettge, T., Buja, L., Kiehl, J.T., Washington, W.M., Fu, Q., Sikka, D.R., Wild, M., 2005. Atmospheric brown clouds: impacts on South Asian climate and hydrological cycle. Proc. Natl. Acad. Sci. U. S. A. 102, 5326–5333.
Ramanathan, V., Li, F., Ramana, M.V., Praveen, P.S., Kim, D., Corrigan, C.E., Nguyen, H., Stone, E.A., Schauer, J.J., Carmichael, G.R., Adhikary, B., Yoon, S.C., 2007. Atmospheric brown clouds: hemispherical and regional variations in long-range transport, absorption, and radiative forcing. J. Geophys. Res. 112, D22S21.
Song, J., Li, M., Jiang, B., Wei, S., Fan, X., Peng, P., 2018. Molecular characterization of water-soluble humic like substances in smoke particles emitted from combustion of biomass materials and coal using ultrahigh-resolution electrospray ionization Fourier transform ion cyclotron resonance mass spectrometry. Environ. Sci. Technol. 52, 2575–2585.
Srinivas, B., Sarin, M.M., 2014. Brown carbon in atmospheric outflow from the Indo-Gangetic Plain: mass absorption efficiency and temporal variability. Atmos. Environ. 89, 835–843.
Srinivas, B., Sarin, M.M., 2019. Brown carbon in the continental outflow to the North Indian Ocean. Environ. Sci.: Processes Impacts 21, 970–987.
Teich, M., van Pinxteren, D., Wang, M., Kecorius, S., Wang, Z., Müller, T., Močnik, G., Herrmann, H., 2017. Contributions of nitrated aromatic compounds to the light absorption of water-soluble and particulate brown carbon in different atmospheric environments in Germany and China. Atmos. Chem. Phys. 17, 1653–1672.
Wang, X., Heald, C.L., Ridley, D.A., Schwarz, J.P., Spackman, J.R., Perring, A.E., Coe, H., Liu, D., Clarke, A.D., 2014. Exploiting simultaneous observational constraints on mass and absorption to estimate the global direct radiative forcing of black carbon and brown carbon. Atmos. Chem. Phys. 14, 10989–11010.
Wang, Y., Hu, M., Lin, P., Tan, T., Li, M., Xu, N., Zheng, J., Du, Z., Qin, Y., Wu, Y., Lu, S., Song, Y., Wu, Z., Guo, S., Zeng, L., Huang, X., He, L., 2019. Enhancement in particulate organic nitrogen and light absorption of humic-like substances over Tibetan plateau due to long-range transported biomass burning emissions. Environ. Sci. Technol. 53, 14222–14232.
Willoughby, A.S., Wozniak, A.S., Hatcher, P.G., 2014. A molecular-level approach for characterizing water-insoluble components of ambient organic aerosol particulates using ultrahigh-resolution mass spectrometry. Atmos. Chem. Phys. 14, 10299–10314.
Wozniak, A.S., Bauer, J.E., Dickhut, R.M., Xu, L., McNichol, A.P., 2012. Isotopic characterization of aerosol organic carbon components over the eastern United States. J. Geophys. Res. 117.
Wozniak, A.S., Bauer, J.E., Sleighter, R.L., Dickhut, R.M., Hatcher, P.G., 2008. Technical Note: Molecular characterization of aerosol-derived water soluble organic carbon using ultrahigh resolution electrospray ionization Fourier transform ion cyclotron resonance mass spectrometry. Atmos. Chem. Phys. 8, 5099–5111.
Wu, G., Ram, K., Fu, P., Wang, W., Zhang, Y., Liu, X., Stone, E.A., Pradhan, B.B., Dangol, P.M., Panday, A., Wan, X., Bai, Z.P., Kang, S., Zhang, Q., Cong, Z., 2019. Water-soluble brown carbon in atmospheric aerosols from Godavari (Nepal), a regional representative of South Asia. Environ. Sci. Technol. 53, 3471–3479.
Xie, M., Chen, X., Hays, M.D., Lewandowski, M., Offenberg, J., Kleindienst, T.E., Holder, A.L., 2017. Light absorption of secondary organic aerosol: composition and contribution of nitroaromatic compounds. Environ. Sci. Technol. 51, 11607–11616.
Xie, M., Chen, X., Holder, A.L., Hays, M.D., Lewandowski, M., Offenberg, J.H., Kleindienst, T.E., Jaoui, M., Hannigan, M.P., 2019. Light absorption of organic carbon and its sources at a southeastern U.S. location in summer. Environ. Pollut. 244, 38–46.
Yan, C., Zheng, M., Bosch, C., Andersson, A., Desyaterik, Y., Sullivan, A.P., Collett, J.L., Zhao, B., Wang, S., He, K., Gustafsson, O., 2017. Important fossil source contribution to brown carbon in Beijing during winter. Sci. Rep. 7, 43182.
Yan, C., Zheng, M., Sullivan, A.P., Bosch, C., Desyaterik, Y., Andersson, A., Li, X., Guo, X., Zhou, T., Gustafsson, Ö., Collett, J.L., 2015. Chemical characteristics and light-absorbing property of water-soluble organic carbon in Beijing: Biomass burning contributions. Atmos. Environ. 121, 4–12.
Zhang, X., Lin, Y.-H., Surratt, J.D., Weber, R.J., 2013a. Sources, composition and absorption ångström exponent of light-absorbing organic components in aerosol extracts from the Los Angeles Basin. Environ. Sci. Technol. 47, 3685–3693.
Zhang, Y., Shao, M., Lin, Y., Luan, S., Mao, N., Chen, W., Wang, M., 2013b. Emission inventory of carbonaceous pollutants from biomass burning in the Pearl River Delta Region, China. Atmos. Environ. 76, 189–199.
Zheng, G., He, K., Duan, F., Cheng, Y., Ma, Y., 2013. Measurement of humic-like substances in aerosols: a review. Environ. Pollut. 181, 301–314.
Zhong, M., Jang, M., 2014. Dynamic light absorption of biomass-burning organic carbon photochemically aged under natural sunlight. Atmos. Chem. Phys. 14, 1517–1525.
Zhu, M., Jiang, B., Li, S., Yu, Q., Yu, X., Zhang, Y., Bi, X., Yu, J., George, C., Yu, Z., Wang, X., 2019. Organosulfur compounds formed from heterogeneous reaction between SO2 and particulate-bound unsaturated fatty acids in ambient air. Environ. Sci. Technol. Lett. 6, 318–322.
Zhu, S., Ding, P., Wang, N., Shen, C., Jia, G., Zhang, G., 2015. The compact AMS facility at Guangzhou Institute of Geochemistry, Chinese Academy of Sciences. Nucl. Instrum. Meth. B 361, 72–75.
Zuth, C., Vogel, A.L., Ockenfeld, S., Huesmann, R., Hoffmann, T., 2018. Ultra-high-resolution mass spectrometry in real-time: atmospheric pressure chemical ionization orbitrap mass spectrometry (APCI-Orbitrap-MS) of atmospheric organic aerosol. Anal. Chem. 90, 8816–8823.